

# Modulation of the thermodynamic, kinetic and magnetic properties of the hydrogen monomer on graphene by charge doping

Liang Feng Huang,<sup>1</sup> Mei Yan Ni,<sup>2</sup> Guo Ren Zhang,<sup>1</sup> Wang Huai Zhou,<sup>1</sup> Yong Gang Li,<sup>1</sup> Xiao Hong Zheng,<sup>1</sup> and Zhi Zeng<sup>1,\*</sup>

<sup>1</sup>*Key Laboratory of Materials Physics, Institute of Solid State Physics,*

*Chinese Academy of Sciences, Hefei 230031, China*

<sup>2</sup>*School of Electronic Science and Applied Physics,*

*Hefei University of Technology, Hefei 230009, China*

## Abstract

The thermodynamic, kinetic and magnetic properties of the hydrogen monomer on doped graphene layers were studied by ab initio simulations. Electron doping was found to heighten the diffusion potential barrier, while hole doping lowers it. However, both kinds of dopings heighten the desorption potential barrier. The underlying mechanism was revealed by investigating the effect of doping on the bond strength of graphene and on the electron transfer and the coulomb interaction between the hydrogen monomer and graphene. The kinetic properties of H and D monomers on doped graphene layers during both the annealing process (annealing time  $t_0 = 300$  s) and the constant-rate heating process (heating rate  $\alpha = 1.0$  K/s) were simulated. Both electron and hole dopings were found to generally increase the desorption temperatures of hydrogen monomers. Electron doping was found to prevent the diffusion of hydrogen monomers, while the hole doping enhances their diffusion. Macroscopic diffusion of hydrogen monomers on graphene can be achieved when the doping-hole density reaches  $5.0 \times 10^{13} \text{ cm}^{-2}$ . The magnetic moment and exchange splitting were found to be reduced by both electron and hole dopings, which was explained by a simple exchange model. The study in this report can further enhance the understanding of the interaction between hydrogen and graphene and is expected to be helpful in the design of hydrogenated-graphene-based devices.

PACS numbers: 68.65.Pq, 67.63.-r, 68.43.Bc

## I. INTRODUCTION

In recent years, there have been many investigations into hydrogenated graphite surfaces and graphene due to their importance in astronomic exploration,<sup>1-4</sup> nuclear industry,<sup>4,5</sup> graphite (graphene)-based hydrogen storage<sup>6</sup> and graphene-based electronic devices.<sup>7-18</sup>

Study of the thermodynamic and kinetic properties of hydrogen adatoms on graphene can help to understand the interaction mechanism between the hydrogen adatom and the graphite surface (graphene layer). The usability of the newly proposed hydrogenated-graphene-based devices relies heavily on these properties. Many experiments have been carried out on the thermodynamic and kinetic properties of hydrogen adatoms on graphite surfaces,<sup>2,3,19,20</sup> substrate-supported graphene layers (monolayer and multilayer)<sup>8,9,11,13,14</sup> and even the free standing graphene layer.<sup>9,21</sup> The hydrogenation of graphene starts with the adsorption of a hydrogen monomer, which breaks an aromatic  $\pi$  bond in graphene and makes the adsorption of other hydrogen atoms very easy. Thus, the thermodynamic and kinetic properties of the hydrogen monomer are essential to the hydrogenation process, which are having been investigated theoretically in recent years.<sup>3,22-28</sup> The ab initio simulation from our previous paper<sup>28</sup> has given some predictions of the kinetic properties of the hydrogen monomer on neutral graphene, which closely reproduced some experimental observations<sup>3,29</sup>. Furthermore, the hydrogen monomer has been used by some theorists to engineer the electronic structures, magnetic properties and transport properties of some graphene-based devices.<sup>30,31</sup> The thermodynamic and kinetic properties of the hydrogen monomer are critical to the stability of these devices.

The charge doping of graphene is a common phenomenon in intercalated graphite compounds,<sup>32-34</sup> metallic surface-supported graphene layers<sup>35-37</sup> and gated graphene layers.<sup>38,39</sup> Charge (electron or hole) doping was expected to influence the thermodynamic and kinetic properties of hydrogen adatoms (including monomers) on graphene. In addition, the magnetism in graphene-based materials has recently drawn tremendous interest from the scientific community due to their lower density compared to transition metals, compatibility with biological systems, plasticity and so on,<sup>40</sup> which introduces another set of applications for charge-doping effects on the hydrogenated graphene. Overall, charge doping provides a possible approach to modifying various properties of hydrogenated-graphene-based materials and devices to fulfill the requirements for various applications.

In this report, the thermodynamic and kinetic properties of the hydrogen monomer on doped

graphene layers were simulated using a composite method consisting of density functional theory (DFT),<sup>41</sup> density functional perturbation theory (DFPT)<sup>42</sup> and harmonic transition state theory (hTST).<sup>43–45</sup> The mechanism of the charge-doping effect on the thermodynamic and kinetic properties of the hydrogen monomer was revealed by investigating the electronic structures and phonon spectra. The kinetic properties of H and D monomers on doped graphene layers during both the annealing process ( $t_0 = 300$  s) and the constant-rate heating (1.0 K/s) were simulated. The effect of charge doping on the magnetic properties derived by DFT calculations have been well explained by a simple exchange model.

## II. METHODOLOGY

The adsorption energy of the hydrogen monomer  $E_{ads}$  is defined as the energy difference between the totally desorbed state and the adsorbed state

$$E_{ads} = E^H + E^{GL} - E^{GL+H} \quad (1)$$

where  $E^H$ ,  $E^{GL}$  and  $E^{GL+H}$  are the total energies of an isolated hydrogen atom, an isolated graphene layer and a graphene layer with a hydrogen monomer adsorbed on it, respectively. Electron doping will make the anti-bonding  $\pi^*$  orbital in graphene occupied by electrons, while hole doping will reduce the electronic occupation of the bonding  $\pi$  orbital. Thus, both the bonding  $\pi$  and the anti-bonding  $\pi^*$  orbitals, which are together described by a total  $\Pi$  bond, are considered here. The chemisorption of a hydrogen monomer will break an aromatic  $\Pi$  bond. The breaking energy of a  $\Pi$  bond ( $E_{\Pi}$ ) is related to the adsorption energy of the hydrogen monomer in the chemisorption state, according to Ferro's analysis.<sup>48</sup> Therefore, a simple model is used to reexpress  $E_{ads}$  as

$$E_{ads}(\sigma) = E_{C-H}(\sigma) - E_{\Pi}(\sigma) \quad (2)$$

where  $\sigma$  is the doping-charge density and  $E_{C-H}(\sigma)$  is the formation energy of a C–H bond. If  $E_{C-H}$  is assumed to be unchanged under charge doping, the contribution of  $E_{\Pi}(\sigma)$  to  $E_{ads}(\sigma)$  is explicitly addressed in this way. The adsorption energy based on this assumption is expressed as

$$E_{ads}^*(\sigma) = E_{C-H}(0) - E_{\Pi}(\sigma) \quad (3)$$

Comparing  $E_{ads}$  in Equ. (2) with  $E_{ads}^*$  in Equ. (3) gives the relative contributions of  $E_{C-H}(\sigma)$  and  $E_{\Pi}(\sigma)$  to  $E_{ads}(\sigma)$ .  $E_{\Pi}$  can be calculated from the adsorption energies of the hydrogen monomer

and para-dimer<sup>48</sup>

$$E_{\Pi}(\sigma) = E_{ads}^{para}(\sigma) - 2E_{ads}(\sigma) \quad (4)$$

where  $E_{ads}^{para}$  is the adsorption energy of a hydrogen para-dimer on graphene.

The over-barrier jump frequency  $\nu$  between two local minimum states (initial and final states or reactant and product states) is calculated from the quantum-mechanically modified hTST,<sup>28,43,46,47</sup> in the Arrhenius form of

$$\nu = \nu_{qm}^* \exp\left(-\frac{E_{ac}}{k_B T}\right) \quad (5)$$

where  $\nu_{qm}^*$  is the exponential prefactor and  $E_{ac}$  is the activation energy. The activation energy  $E_{ac}$  is defined as the vibrational zero-point energy corrected potential barrier, which is expressed as

$$\begin{aligned} E_{ac} &= \Delta V_p + \frac{1}{2} \sum_{i=1}^{3N-1} \hbar\omega_i^S - \frac{1}{2} \sum_{i=1}^{3N} \hbar\omega_i^I \\ &= \Delta V_p - \Delta F_{vib}(0) \end{aligned} \quad (6)$$

where  $\Delta V_p$  is the potential barrier in the reaction path, which can be obtained from DFT calculations;  $\omega_i^I$  and  $\omega_i^S$  are the vibrational frequencies of the  $i$ th mode in the initial and saddle-point (SP) states, respectively, which can be obtained from DFPT calculations;  $\Delta F_{vib}(0)$  is the vibrational zero-point energy correction. The total vibrational degrees of freedom are  $3N$ . An imaginary vibrational mode along the migration coordinate in the SP state is excluded from calculation. Thus, there are  $3N-1$  vibrational modes considered for the SP state. The quantum-mechanically modified prefactor is expressed as<sup>28</sup>

$$\nu_{qm}^* = \frac{k_B T}{h} \frac{\prod_{i=1}^{3N-1} \exp\left(\frac{\hbar\omega_i^S}{k_B T}\right) \bar{n}_T(\omega_i^S)}{\prod_{i=1}^{3N} \exp\left(\frac{\hbar\omega_i^I}{k_B T}\right) \bar{n}_T(\omega_i^I)} \quad (7)$$

where  $\bar{n}_T(\omega_i)$  is the bosonic phonon occupation number of the  $i$ th vibrational mode.

The first-order rate equation for the desorption of the hydrogen monomer is defined as<sup>28,29,44</sup>

$$\frac{dn(t)}{dt} = -\nu_{des}(T)n(t) \quad (8)$$

where  $\nu_{des}$  is the desorption jump frequency of the hydrogen monomer;  $n(t)$  is the residual number of hydrogen monomers on a graphene layer at time  $t$ ;  $t = 0$  represents the starting time of the kinetic movement.

In the annealing process ( $T = T_0$ ), the variation of the residual number with respect to the annealing time interval ( $t_0$ ) is expressed as

$$n(t) = n(0) \exp[-v_{des}(T_0)t_0] \quad (9)$$

where  $n(0)$  is the monomer number at the starting time ( $t = 0$ ). Conceptually, the relative residual monomer number ( $n(t)/n(0)$ ) is also the desorption probability of a single monomer. In this case, the diffusional property can be described by the mean square displacement ( $\langle |\mathbf{r}(t) - \mathbf{r}(0)|^2 \rangle$ ) of a monomer parallel to the graphene layer. From Fick's second law, we have

$$\langle |\mathbf{r}(t) - \mathbf{r}(0)|^2 \rangle = 2dD_{ad}(T_0)t_0 \quad (10)$$

where  $d$  is the dimensionality of the diffusion of a hydrogen monomer on graphene, taken to be 2 here, and  $D_{ad}$  is the temperature-dependent diffusion coefficient of the adatom, described by<sup>46</sup>

$$D_{ad} = \frac{1}{2d} \Gamma a^2 \quad (11)$$

where  $\Gamma$  is the total jump frequency of the monomer, and  $a$  is the jump length. For the diffusion of a hydrogen monomer on graphene,  $\Gamma$  is taken as  $3v_{diff}$  ( $v_{diff}$  is the diffusion jump frequency) because there are three equivalent paths for the diffusion of a monomer on graphene, and  $a$  is taken as the optimized C–C bond length of 1.426 Å. The diffusion radius of the monomer is defined as the square root of the mean square displacement

$$r_{dif} = \sqrt{2dD_{ad}(T_0)t} \quad (12)$$

which directly determines the diffusional mobility of the hydrogen monomer on graphene.

In the constant-rate heating process ( $T = \alpha t$ ), the variation of the residual number with respect to time is

$$n(t) = n(0) \exp\left[-\int_0^t v_{des}(T)dt\right] \quad (13)$$

where the heating rate  $\alpha$  is always taken as 1.0 K/s in experiments.<sup>2,19,20</sup> In this case, the diffusion radius is expressed as

$$r_{dif} = \sqrt{2d \int_0^t D_{ad}(T)dt} \quad (14)$$

In this study, a hydrogen monomer on a  $5 \times 5$  periodic supercell of graphene (50 C atoms), with a 10 Å vacuum along the direction perpendicular to the surface, was taken as an isolated monomer.

The DFT and DFPT calculations were carried out using the Quantum Espresso code package.<sup>49</sup> The ultrasoft<sup>50</sup> spin-polarized PBE<sup>51</sup> pseudopotentials were applied to describe the electronic exchange and correlation energy. The reaction path was described by the minimum energy path (MEP) between two local minimum states (Fig. 1), and the MEPs for the desorption and diffusion of a hydrogen monomer on graphene were calculated using the climbing-image nudged elastic band method.<sup>52</sup> For calculating the vibrational frequencies of the periodic supercells, only the gamma point at the Brillouin zone center is selected. The charge-doped systems were compensated with the same numbers of opposite background charges. The optimized C–C bond length of graphene is 1.426 Å; thus, a charge density of  $1.0 \times 10^{13} \text{ cm}^{-2}$  corresponds to a charge number of 0.1314  $e$  added into the graphene supercell. More details about the computational method and tests can be found in Ref. [28].

### III. RESULTS AND DISCUSSION

Schematic drawings of the MEPs for the desorption and diffusion processes of a hydrogen monomer on graphene are shown in Fig. 1, where the structures of the initial (reactant), SP (transition) and final (product) states are also shown. The initial state is the chemisorption state, and the final state here is set as the physisorption state. The potential barrier is the energy difference between the SP state and the initial state. The variation of the adsorption energy of the hydrogen monomer in the initial state ( $E_{ads}^I$ ), diffusion SP state ( $E_{ads}^{dif,S}$ ) and desorption SP state ( $E_{ads}^{des,S}$ ), and of the potential barriers for the desorption ( $\Delta V_p^{des}$ ) and diffusion ( $\Delta V_p^{dif}$ ) of the hydrogen monomer with respect to the doping-charge density ( $\sigma$ ) are shown in Fig. 2.

$E_{ads}^I$  increases with the number of doping electrons (negative charge) or doping holes (positive charge). However, the curve of  $E_{ads}^I$  is asymmetric about  $\sigma = 0.0$ , because the rate of increase is greater under hole doping than under electron doping.  $E_{ads}^{dif,S}$  increases monotonically with increasing  $\sigma$  from negative to positive, and the rate of increase becomes larger than that of  $E_{ads}^I$  under hole doping, but smaller under electron doping. The curve of  $E_{ads}^{des,S}$  is somewhat flat compared with those of  $E_{ads}^I$  and  $E_{ads}^{dif,S}$ . The potential barrier of diffusion  $\Delta V_p^{dif}$  ( $= E_{ads}^I - E_{ads}^{dif,S}$ ) decreases monotonically with increasing  $\sigma$  from negative to positive, while the potential barrier of desorption  $\Delta V_p^{des}$  ( $= E_{ads}^I - E_{ads}^{des,S}$ ) increases with the number of doping electrons or holes. These phenomena in energy are related to the electronic structure of graphene and to the electron transfer and coulomb interaction between the hydrogen monomer and graphene, which will be explained

in detail below.

The band structure of neutral graphene is shown in Fig. 3(a), where the anti-bonding  $\pi^*$  band is above the Fermi level and the bonding  $\pi$  band is below the Fermi level. The anti-bonding and bonding characteristics of the  $\pi^*$  and  $\pi$  bands are shown by their orbital shapes in real space in Fig. 3(b) and (c), respectively. Upon electron doping, the Fermi level goes up, leading to the occupation of the anti-bonding  $\pi^*$  band, and the strength of the total  $\Pi$  bond is weakened. Upon hole doping, the Fermi level goes down, reducing the electron-occupation number in the bonding  $\pi$  band, and thus the strength of the  $\Pi$  bond is also weakened. The  $E_{\Pi}$  obtained at different  $\sigma$  by Equ. 4 are shown in Fig. 2(a).  $E_{\Pi}$  decreases with increasing the number of doping electrons or holes, inverse to the variation of  $E_{ads}^I$ . This is consistent with the weakening of the  $\Pi$  bond predicted from the electronic structure of graphene. The curve of  $E_{\Pi}$  is asymmetric because the rate of decrease is greater under hole doping than under electron doping, like the variation of  $E_{ads}^I$ . From Equ. 2 and 3, the weakening of the  $\Pi$  bond, namely the decrease of  $E_{\Pi}$ , results in the increase of  $E_{ads}^I$  and  $E_{ads}^*$ , both of which exhibit a similar trend (Fig. 2(a)). However, the general lower value of  $E_{ads}^I$  than that of  $E_{ads}^*$  indicates the effect of the charge doping on  $E_{C-H}$ , which is related to the electron transfer and coulomb interaction between the hydrogen monomer and the doped graphene (shown below).

The calculated Löwdin electronic populations, also called the *net atomic population* by Mulliken,<sup>53</sup> of the hydrogen monomer ( $N_e^H$ ) in the initial, diffusion SP and desorption SP states are shown in Fig. 4.  $N_e^H$  decreases monotonically with increasing  $\sigma$  from negative to positive. The  $N_e^H$ s for the initial state are smaller than 1.0 due to the electron transfer from the hydrogen monomer to graphene, mainly through the orbital hybridization between them. This orbital hybridization in the initial state will be shown later to be unchanged by the charge doping. However, the electron transfer is still influenced by charge doping due to the chemical-potential difference between the hybridized hydrogen monomer and graphene. The monotonic decrease of  $N_e^H$  for the initial state indicates that the electron doping tends to block but the hole doping to promote the electron transfer from the adsorbed hydrogen monomer to graphene. This blockage of electron transfer under electron doping tends to reduce the affinity of graphene to bond with the hydrogen monomer, so that  $E_{C-H}$  decreases with increasing doping electrons, making  $E_{ads}^I < E_{ads}^*$  under electron doping (by Equ. (2) and (3)). On the other hand, hole doping tends to promote electron transfer so as to increase  $E_{C-H}$ , making  $E_{ads}^I$  a little larger than  $E_{ads}^*$  at  $\sigma \lesssim 2.5 \times 10^{13} \text{ cm}^{-2}$ . However, at  $\sigma > 2.5 \times 10^{13} \text{ cm}^{-2}$ , the further promoted electron transfer increases the coulomb repulsion

between the positively charged hydrogen monomer and the hole-doped graphene, which weakens the strength of the C–H bond and makes  $E_{ads}^I < E_{ads}^*$  again. The weakening of the strength of the C–H bond by charge doping can also be qualitatively observed from the variation of its bond length ( $d_{C-H}$ ) under charge doping in Fig. 5. The variation of the protrusion height of the H-bonded C atom ( $Z_{C^*}$ ) with  $\sigma$  is also shown in Fig. 5, which will be used later. It should be noted that the increase of  $E_{ads}^I$  by charge doping is mainly determined by the reduction of the breaking energy of a total  $\Pi$  bond ( $E_{\Pi}$ ), as described in detail in the previous paragraph, and the electron transfer and coulomb repulsion play minor roles. However, from the electronic density of states (DOS) of the neutral desorption and diffusion SP states as described in Ref. 28, the hydrogen monomer hybridizes little with graphene. This is the same for these doped cases, but only with Fermi levels tuned by charge doping (not shown). Thus,  $E_{ads}^{des,S}$  and  $E_{ads}^{dif,S}$  should be not significantly related to  $E_{\Pi}$ . The  $N_e^H$ s for the desorption SP state are larger than 1.0 under electron doping and smaller than 1.0 under hole doping. The doping charges distribute across the system according to the requirement of electrostatic equilibrium, which explains the flatness of the  $E_{ads}^{des,S}(\sigma)$  curve in Fig. 2(a). The  $N_e^H$ s for the diffusion SP state are significantly smaller than 1.0. From the DOS in Ref. 28, the hydrogen monomer will dope graphene with some number of itinerant electrons in this state. The monotonic decrease of  $N_e^H$  (promotion of the electron transfer) with increasing  $\sigma$  is due to the chemical-potential difference between the hydrogen monomer and doped graphene, which is the same as the electronic population of the lithium adatom on charged carbon nanotubes.<sup>54</sup> This promotion of electron transfer results in the increase of the affinity of graphene to bond with the hydrogen monomer in the diffusion SP state and results in the increase of  $E_{ads}^{dif,S}$ . As a result, the increase of  $\Delta V_p^{des} (= E_{ads}^I - E_{ads}^{des,S})$  under charge (electron or hole) doping and the monotonic decrease of  $\Delta V_p^{dif} (= E_{ads}^I - E_{ads}^{dif,S})$  with increasing  $\sigma$  are conjunctly due to the effects of charge doping on the strength of the total  $\Pi$  bond of graphene, the electron transfer and to the coulomb interaction between the hydrogen monomer and graphene.

The calculated vibrational zero-point energy corrections ( $\Delta F_{vib}(0)$ ) for the desorption and diffusion of H and D monomers under various  $\sigma$ s are shown in Fig. 6. The isotope effect of  $\Delta F_{vib}(0)$  is obvious; it decreases with increasing monomer mass. This will result in the reversed isotope effect in the activation energy by Equ. 6.  $\Delta F_{vib}(0)$  and its isotopic difference for desorption are generally larger than those for diffusion. These vibrational properties are related to the spectra of the localized vibrational modes of H and D monomers, which has been discussed in detail in Ref. 28. The  $\Delta F_{vib}(0)$ s for the diffusion of H and D monomers decrease with increasing  $\sigma$ , the same



as  $\Delta V_p^{dif}$ . This is because the decrease of the potential barrier  $\Delta V_p^{dif}$  will result in the decrease of the diffusion-MEP potential curvature around the initial state, which then results in the lowering of the frequencies of the effective vibrations for the diffusion of H and D monomers whose zero-point energies equal their  $\Delta F_{vib}(0)$ s. Except for the kinks at  $\sigma$  of  $-5.0 \times 10^{13} \text{ cm}^{-2}$ , the  $\Delta F_{vib}(0)$ s for the desorption of H and D monomers present the same variation as  $\Delta V_p^{des}$  with respect to  $\sigma$ , which is that the values increase with the number of doping electrons or holes. This is related to the increase of the potential barrier of the desorption-MEP and the increase of the frequencies of effective vibrations for the desorption of H and D monomers. The kinks in the  $\Delta F_{vib}(0)$  curves for the desorption of H and D monomers at  $\sigma$  of  $-5.0 \times 10^{13} \text{ cm}^{-2}$  are related to the structure of the desorption SP state. The protrusion height of the H-bonded  $C^*$  ( $Z_{C^*}$ ) in the chemisorption and SP states can be used to determine the structural information. It can be seen in Fig. 5, there is an obvious kink in the  $Z_{C^*}(\sigma)$  curve for the desorption SP state at  $\sigma = -5.0 \times 10^{-13} \text{ cm}^{-2}$ , while the  $Z_{C^*}(\sigma)$  curves for the initial and diffusion SP states are much smoother. This kink makes the  $C^*$  closer to the hydrogen monomer in the desorption SP state at  $\sigma = -5.0 \times 10^{-13} \text{ cm}^{-2}$  than at other charge densities. Then, the interaction between hydrogen monomer and graphene in the desorption SP state at  $\sigma = -5.0 \times 10^{-13} \text{ cm}^{-2}$  will be larger than at other charge densities, which also can be reflected in the spectra of the localized vibrational modes of the hydrogen monomer (shown below).

The localized vibrational modes have large displacements ( $\mathbf{e}(\omega_i)$ ,  $i$  is the index of the vibrational mode) of the hydrogen monomer in their eigenvectors of the vibrational dynamic matrix. The spectra of  $|\mathbf{e}(\omega_i)|^2$  for the initial and desorption SP states at  $\sigma$ s of  $-5.0 \times 10^{13}$  and  $-7.5 \times 10^{13} \text{ cm}^{-2}$  are shown in Fig. 7. The stretching (S) modes become imaginary in the desorption SP states. Compared with the bending (B) modes in the initial states, the bending modes in the desorption SP states are much less lowered at  $\sigma$  of  $-5.0 \times 10^{13} \text{ cm}^{-2}$  than at  $\sigma$  of  $-7.5 \times 10^{13} \text{ cm}^{-2}$ . The phonon spectra at other  $\sigma$ s (e.g. see the Fig. 3 in Ref. 28 for the neutral case) are close to those at  $\sigma$  of  $-7.5 \times 10^{13} \text{ cm}^{-2}$  and shift smoothly with  $\sigma$ , which is also reflected by the  $\Delta F_{vib}(0)$  curves (Fig. 6). As described in the previous paragraph, the interaction between the hydrogen monomer and graphene in the desorption SP state at  $\sigma$  of  $-5.0 \times 10^{13} \text{ cm}^{-2}$  is larger than those at other  $\sigma$ s, and thus (the absolute values of) the vibrational frequencies of the localized vibrational modes of the hydrogen monomer are higher at this  $\sigma$  than those at other  $\sigma$ s. By Equ. 6, the result is that the  $\Delta F_{vib}(0)$ s for the desorption SP state are lower at  $\sigma$  of  $-5.0 \times 10^{13} \text{ cm}^{-2}$  than at other  $\sigma$ s, and that the  $E_{ac}$ s for desorption at  $\sigma$ s of  $-5.0$  and  $-7.5 \times 10^{13} \text{ cm}^{-2}$  are very close to each other. By Equ.

7 and from the detailed analysis in Ref. 28, the stiffening of the localized vibrational modes in the desorption SP state at  $\sigma$  of  $-5.0 \times 10^{13} \text{ cm}^{-2}$  will also result in the decrease of the corresponding  $v_{qm}^*$ s compared with those at other  $\sigma$ s.

The calculated jump frequencies ( $\nu$ ) for the desorption and diffusion of H and D monomers on doped graphene are shown in Fig. 8. The value of  $\nu$  decreases with increasing monomer mass. This isotope effect is due to the isotope effect in  $\Delta F_{vib}(0)$  (Fig. 6) by Equ. 5 and 6, which has been discussed in detail in Ref. 28. In Fig. 8(a) and (b), the desorption  $\nu$  generally decreases with increasing the number of doping electrons (negative  $\sigma$ ) or holes (positive  $\sigma$ ), with the exception that the  $\nu$  for the desorption of H (D) monomer at  $\sigma$  of  $-5.0 \times 10^{13} \text{ cm}^{-2}$  is less than that at  $\sigma$  of  $-7.5 \times 10^{13} \text{ cm}^{-2}$ . By Equ. 5,  $\nu$  is exponentially determined by  $E_{ac}(\sigma)$  ( $= \Delta V_p^{des} + \Delta F_{vib}(0)$ ), where the linear dependence on  $v_{qm}^*$  usually plays a minor role. Except at  $\sigma$  of  $-5.0 \times 10^{13} \text{ cm}^{-2}$ , the  $E_{ac}$  for the desorption of H (D) monomer increases with the number of doping electrons or holes; thus, the desorption  $\nu$  generally decreases with increasing the number of doping electrons or holes. However, the lowering of the  $\Delta F_{vib}(0)$ s at  $\sigma$  of  $-5.0 \times 10^{13} \text{ cm}^{-2}$  makes the  $E_{ac}$ s very close to those at  $\sigma$  of  $-7.5 \times 10^{13} \text{ cm}^{-2}$ , and the relative magnitudes of the  $\nu$ s at these two charge densities are determined by the values of their  $v_{qm}^*$ s. The  $v_{qm}^*$  at  $\sigma$  of  $-5.0 \times 10^{13} \text{ cm}^{-2}$  is smaller than those at other  $\sigma$ s due to the stiffening of the localized modes (not shown), as described in the previous paragraph. In Fig. 8(c), the diffusion  $\nu$  increases monotonically with  $\sigma$ , which is due to the monotonic decrease of  $E_{ac}$  for diffusion with increasing  $\sigma$ . Thus, it can be concluded that any kind of charge (electron or hole) doping will make the bonding between the hydrogen monomer and graphene kinetically more stable, and electron doping will prevent but the hole doping will trigger the diffusion of the hydrogen monomer on graphene. Thus, when increasing  $\sigma$  from negative to positive, there should be a crossover between the priorities of desorption and diffusion of H (D) monomer on graphene, like the crossover between  $\Delta V_p^{des}$  and  $\Delta V_p^{dif}$  in Fig. 2.

In the annealing process, the system is kept at an annealing temperature ( $T_0$ ) for a fixed time interval ( $t_0$ ). In the simulation here of the kinetic properties of H and D monomers in the annealing process,  $t_0$  was set to be 300s. For electron-doped graphene layers, only the desorption of the hydrogen monomer was considered in the simulation, because the diffusion is stopped by electron doping. However, for hole-doped graphene layers, both the desorption and the diffusion of the hydrogen monomer were considered. The properties of desorption and diffusion can be characterized by the relative residual monomer number (or the desorption probability) ( $n(t_0)/n(0)$ ) and the diffusion radius ( $r_{dif}(t_0)$ ), respectively. The calculated variations of the  $n(t_0)/n(0)$ s and  $r_{dif}(t_0)$ s of

H and D monomers at various  $\sigma$ s with respect to  $T_0$  are shown in Fig. 9. At  $n(t_0)/n(0) = 0.5$ , the corresponding  $T_0$  was defined to be the desorption temperature. The desorption temperature of H (D) on neutral graphene is 282 (301) K. Under electron doping, the desorption temperatures of H (D) monomer are 295 (314), 333 (349) and 330 (348) K at  $\sigma$ s of  $-2.5$ ,  $-5.0$  and  $-7.5 \times 10^{13} \text{ cm}^{-2}$ , respectively. Under hole doping, the desorption temperatures are 313 (331), 359 (376) and 407 (424) K at  $\sigma$ s of  $2.5$ ,  $5.0$  and  $7.5 \times 10^{13} \text{ cm}^{-2}$ , respectively. The desorption temperatures for D monomer are about 18 K higher than those for H monomer. The  $r_{dif}$  of H (D) monomer on neutral graphene at the desorption temperature is 0.6 (1.0) Å, which is smaller than the C–C bond length of 1.426 Å and indicates the immobility of the hydrogen monomer in diffusion. Under hole doping, the  $r_{difs}$  of H (D) monomer at the desorption temperatures are 9.0 (12.5) nm, 0.65 (0.71)  $\mu\text{m}$  and 10.7 (9.8)  $\mu\text{m}$  at  $\sigma$ s of  $2.5$ ,  $5.0$  and  $7.5 \times 10^{13} \text{ cm}^{-2}$ , respectively. The isotope effect on the desorption and diffusion of the hydrogen monomer can be concluded to be that the lighter hydrogen monomer is desorbed and diffuses more easily. The variations of the desorption temperatures and  $r_{difs}$  with respect to  $\sigma$  are the same as those of the  $v$ s for desorption and diffusion, respectively. If diffusion with radius above 0.1  $\mu\text{m}$  is defined to be macroscopic diffusion, the macroscopic diffusion of H (D) monomer at temperatures below the desorption temperature can be achieved when  $\sigma$  reaches  $5.0 \times 10^{13} \text{ cm}^{-2}$ .

In the constant-rate heating process, the system is heated at a constant rate ( $T = \alpha t$ ). The heating rate ( $\alpha$ ) was taken to be 1.0 K/s in the simulation here, which was a commonly used value in experiments. The calculated variations of the  $n(t_0)/n(0)$ s and  $r_{dif}(t_0)$ s at various  $\sigma$ s are shown in Fig. 10. The desorption temperature of H (D) on neutral graphene is 313 (333) K. Under electron doping, the desorption temperatures of H (D) monomer are 326 (346), 367 (384) and 363 (382) K at  $\sigma$ s of  $-2.5$ ,  $-5.0$  and  $-7.5 \times 10^{13} \text{ cm}^{-2}$ , respectively. Under hole doping, the desorption temperatures are 345 (363), 394 (412) and 445 (461) K at  $\sigma$ s of  $2.5$ ,  $5.0$  and  $7.5 \times 10^{13} \text{ cm}^{-2}$ , respectively. The desorption temperatures in the constant-rate heating process are about 33 K higher than those in the annealing process. The desorption temperatures for D monomer are also about 18 K higher than those for H monomer. The  $r_{dif}$  of H (D) monomer on neutral graphene at the desorption temperature is 0.8 (1.3) Å, which is also smaller than the C–C bond length and indicates the immobility of the hydrogen monomer in diffusion. Under hole doping, the  $r_{difs}$  of H (D) monomer at the desorption temperatures are 7.5 (9.6) nm, 0.41 (0.41)  $\mu\text{m}$  and 5.9 (5.6)  $\mu\text{m}$  at  $\sigma$ s of  $2.5$ ,  $5.0$  and  $7.5 \times 10^{13} \text{ cm}^{-2}$ , respectively. The isotope effect on the desorption and diffusion of the hydrogen monomer on graphene and the variations of the desorption temperatures and the

$r_{difs}$  with respect to  $\sigma$  are the same as those in the annealing process. The macroscopic diffusion of the hydrogen monomer is also achieved in this constant-rate heating process when  $\sigma$  reaches  $5.0 \times 10^{13} \text{ cm}^{-2}$ .

Although the diffusion radius can be increased by hole doping, the hydrogen monomer on heavily hole-doped graphene layers may not be easily observed in experiments, because highly diffusive hydrogen monomers tend to meet and form hydrogen dimers and clusters, which are much more stable than isolated monomers,<sup>3</sup> or quickly diffuse to the edge of the finite-sized sample. Thus, to observe the diffusion of a hydrogen monomer experimentally, a medium hole density was suggested. The hydrogen monomer on suspended graphene sheet has been detected to be stable by transmission electron microscopy (TEM) at room temperature.<sup>21</sup> Although this stability may be due to the low actual sample temperature caused by the cold trap used in the experiment, the effect of the incident electrons in TEM should also be considered. The incident electrons will inevitably excite the electrons in the bonding  $\pi$  band up to the anti-bonding  $\pi^*$  band in graphene. This excitation reduces the electronic occupation number of the  $\pi$  band and increases that of the  $\pi^*$  band together, which weakens the total  $\Pi$  bond in graphene and enhances the stability of the hydrogen monomer on graphene, according to the analysis above.

The adsorption of hydrogen monomer onto neutral graphene can break an aromatic  $\pi$  bond, which results in two dangling  $C(p_z)$  orbitals. Then, one  $C(p_z)$  orbital bonds with the  $H(1s)$  orbital, and the  $C(p_z)$  orbital left unsaturated forms an occupied spin-polarized quasilocal state (spin-up) around the hydrogen monomer.<sup>23,28,55</sup> In the spectrum of the electronic DOS (Fig. 11), the occupied quasilocal state presents as a narrow spin-up peak within the gap between the conduction and valence bands, and there is another narrow peak above the Fermi energy ( $E_F$ ) that corresponds to the unoccupied spin-down quasilocal state. The energy difference between these two peaks is due to the exchange interaction of electrons, and this exchange splitting in energy was defined as  $\Delta_s$ . The electronic occupation number of these two quasilocal states can be changed by charge doping. The calculated DOS of the chemisorption state at various  $\sigma$ s are shown in Fig. 11. The contribution of the  $H(1s)$  orbital to the total DOS (not shown) does not significantly vary with charge doping, and is nearly the same as that in the neutral case in Ref. 28, which indicates that charge doping does not significantly influence the orbital hybridization between the hydrogen monomer and graphene. This can also be validated from the invariance of the gap of 1.29 eV between the conduction and valence bands with respect to  $\sigma$ . It can be seen that  $\Delta_s$  decreases with increasing  $|\sigma|$ . The electronic occupation numbers of the lower spin-up and the higher spin-down

quasilocal states were defined as  $n^+$  and  $n^-$ , respectively. It can be seen that under electron doping ( $\sigma < 0.0$ ), the spin-up and spin-down quasilocal states are fully and partially occupied ( $n^+ = 1.0$ ,  $n^- < 1.0$ ), respectively, while under hole doping ( $\sigma > 0.0$ ), they are partially and not occupied ( $n^+ < 1.0$ ,  $n^- = 0.0$ ), respectively. The variations of  $\Delta_s$  and  $\Delta n (= n^+ - n^-)$  with respect to  $\sigma$  are shown in Fig. 12. The curve of  $\Delta_s(\sigma)$  is strictly linear and symmetric around  $\sigma = 0.0$ . A simple exchange model can be used to express  $\Delta_s$  as

$$\Delta_s = \epsilon^- - \epsilon^+ = -J_{eff}^- n_- S^- S^- - (-J_{eff}^+) n_+ S^+ S^+ \quad (15)$$

where  $\pm$  represent spin-up and spin-down quasilocal states, respectively;  $\epsilon^\pm$  are the energies of the quasilocal states;  $J_{eff}^\pm$  are the exchange constants;  $S^\pm = \pm \frac{1}{2}$ . In the exchange model, electrons with opposite spins do not interact with each other. The linearity and symmetry of the curve of  $\Delta_s(\sigma)$  indicate that the exchange constant does not vary with the spin orientation or  $\sigma$ , which can be expressed as  $J_{eff}^+(\sigma) = J_{eff}^-(\sigma) = J_{eff}$ . Then, Equ. 15 can be rewritten as

$$\Delta_s = \frac{1}{4} J_{eff} \Delta n \quad (16)$$

The magnetic moment of the system equals  $\Delta n \mu_B$ . The curve  $\Delta_s(\sigma)$  can be well fitted by Equ. 16 with  $J_{eff}$  taken to be 1.23 eV, as shown in Fig. 12.

#### IV. CONCLUSIONS

The thermodynamic and kinetic properties of H and D monomers on doped graphene layers were studied using a composite method consisting of density functional theory, density functional perturbation theory and harmonic transition state theory. The calculated results were analyzed with reference to the electronic structures and phonon spectra. Electron doping has been found to heighten the diffusion potential barrier, while hole doping lowers it. However, both kinds of dopings heighten the desorption potential barrier. These phenomena in energies have been found to be conjunctly due to the effects of charge doping on the strength of the  $\Pi$  bond (defined to include the  $\pi$  and  $\pi^*$  bonds) in graphene and to the electron transfer and the coulomb interaction between the hydrogen monomer and graphene. It has been found that hole doping is necessary for the observation of the diffusion of H and D monomers on graphene. The kinetic properties of H and D monomers on doped graphene layers during both the annealing process ( $t_0 = 300$  s) and the constant-rate heating process ( $\alpha = 1.0$  K/s) were simulated. H monomer is more mobile

than D monomer in the kinetic simulations. Generally, both electron doping and hole doping can increase the desorption temperatures of hydrogen monomers. However, the diffusion of hydrogen monomers is prevented by the electron doping and triggered by the hole doping, and the diffusion radius increases with  $\sigma$  under hole doping. It has been found that the macroscopic diffusion of hydrogen monomers can be achieved at temperatures below the desorption temperature when  $\sigma$  reaches  $5.0 \times 10^{13} \text{ cm}^{-2}$  in graphene. The effect of charge doping on the magnetic properties of the hydrogenated graphene were also studied. The exchange splitting of the spin-up and spin-down quasilocal states and the magnetic moment decrease linearly with the number of doped electrons (holes). The variation of the exchange splitting with respect to  $\sigma$  has been explained by a simple exchange model, where the exchange constant has been found not to vary with the spin orientation or the doping charge density.

### Acknowledgments

The first author (Huang) wishes to thank Liv Horkekær for helpful email exchanges. This work was supported by the special Funds for Major State Basic Research Projects of China (973) under grant No. 2007CB925004, 863 Project, Knowledge Innovation Program of Chinese Academy of Sciences and by Director Grants of CASHIPS. Part of the calculations were performed at the Center of Computational Science of CASHIPS and at the Shanghai Supercomputer Center.

---

\* Email: zzenq@theory.issp.ac.cn

<sup>1</sup> J. M. D. Coey, M. Venkatesan, C. B. Fitzgerald, A. P. Douvalis, and I. S. Sanders, *Nature* **420**, 156 (2002).

<sup>2</sup> L. Hornekær, Ž. Šljivančanin, W. Xu, R. Otero, E. Rauls, I. Stensgaard, E. Lægsgaard, B. Hammer, and F. Besenbacher, *Phys. Rev. Lett.* **96**, 156104 (2006).

<sup>3</sup> L. Hornekær, E. Rauls, W. Xu, Ž. Šljivančanin, R. Otero, I. Stensgaard, E. Lægsgaard, B. Hammer, and F. Besenbacher, *Phys. Rev. Lett.* **97**, 186102 (2006).

<sup>4</sup> Y. Ferro, F. Marinelli, and A. Allouche, *Chem. Phys. Lett.* **368**, 609 (2003).

<sup>5</sup> J. Morris, *Nature* **422**, 674 (2003).

<sup>6</sup> A. J. Lachawiec, Jr., G. Qi, and R. T. Yang, *Langmuir* **21**, 11418 (2005).

- <sup>7</sup> A. V. Shytov, D. A. Abanin, and L. S. Levitov, *Phys. Rev. Lett.* **103**, 016806 (2009).
- <sup>8</sup> S. Ryu, M. Y. Han, J. Maultzsch, T. F. Heinz, P. Kim, M. L. Steigerwald, and L. E. Brus, *Nano Lett.* **8**, 4597 (2008).
- <sup>9</sup> D. C. Elias, R. R. Nair, T. M. G. Mohiuddin, S. V. Morozov, P. Blake, M. P. Halsall, A. C. Ferrari, D. W. Boukhvalov, M. I. Katsnelson, A. K. Geim, and K. S. Novoselov, *Science* **323**, 610 (2009).
- <sup>10</sup> J. O. Sofo, A. S. Chaudhari, and G. D. Barber, *Phys. Rev. B* **75**, 153401 (2007).
- <sup>11</sup> R. Balog, B. Jorgensen, J. Wells, E. Lægsgaard, P. Hofmann, F. Besenbacher, and L. Hornekær, *J. Am. Chem. Soc.* **131**, 8744 (2009).
- <sup>12</sup> A. Bostwick, J. McChesney, K. V. Emtsev, T. Seyller, K. Horn, S. D. Kevan, and E. Rotenberg, *Phys. Rev. Lett.* **103**, 056404 (2009).
- <sup>13</sup> N. P. Guisinger, G. M. Rutter, J. N. Crain, P. N. First, and J. A. Stroscio, *Nano Lett.* **9**, 1462 (2009).
- <sup>14</sup> Z. Luo, T. Yu, K. Kim, Z. Ni, Y. You, S. Lim, and Z. Shen, *ACS Nano* **3**, 1781 (2009).
- <sup>15</sup> S. Lebégue, M. Klintenberg, O. Eriksson, and M. I. Katsnelson, *Phys. Rev. B* **79**, 245117 (2009).
- <sup>16</sup> L. Chen, Z. Ma, and C. Zhang, *Appl. Phys. Lett.* **96**, 023107 (2010).
- <sup>17</sup> A. R. Wright, T. E. O'Brien, D. Beaven, and C. Zhang, *Appl. Phys. Lett.* **97**, 043104 (2010).
- <sup>18</sup> M. Z. S. Flores, P. A. S. Autreto, S. B. Legoas, and D. S. Galvao, *Nanotechnology* **20**, 465704 (2009).
- <sup>19</sup> T. Zecho, A. Güttler, and J. Küppers, *Carbon* **42**, 609 (2004).
- <sup>20</sup> T. Zecho, A. Güttler, X. Sha, B. Jackson, and J. Küppers, *J. Chem. Phys.* **117**, 8486 (2002).
- <sup>21</sup> J. C. Meyer, C. O. Girit, M. F. Crommie, and A. Zettl, *Nature* **454**, 319 (2008).
- <sup>22</sup> Y. Ferro, F. Marinelli, A. Jelea, and A. Allouche, *J. Chem. Phys.* **120**, 11882 (2004).
- <sup>23</sup> S. Casolo, O. M. Løvvik, R. Martinazzo, and C. Franco Tantardini, *J. Chem. Phys.* **130**, 054704 (2009).
- <sup>24</sup> C. P. Herrero and R. Ramírez, *Phys. Rev. B* **79**, 115429 (2009).
- <sup>25</sup> T. Roman, W. A. DiÑo, H. Nakanishi, H. Kasai, T. Sugimoto, and K. Tange, *Japanese Journal of Applied Physics* **45**, 1765 (2006).
- <sup>26</sup> D. W. Boukhvalov, M. I. Katsnelson, and A. I. Lichtenstein, *Phys. Rev. B* **77**, 035427 (2008).
- <sup>27</sup> D. W. Boukhvalov and M. I. Katsnelson, *J. Phys.: Condens. Matter* **21**, 344205 (2009).
- <sup>28</sup> L. F. Huang, M. Y. Ni, X. H. Zheng, W. H. Zhou, Y. G. Li, and Z. Zeng, to be published in *J. Phys. Chem. C*.
- <sup>29</sup> S. Baouche, G. Gamborg, V. V. Petrunin, A. C. Luntz, and A. Baurichter, *J. Chem. Phys.* **125**, 084712 (2006).
- <sup>30</sup> J. Bang and K. J. Chang, *Phys. Rev. B* **81**, 193412 (2010).

- <sup>31</sup> D. Soriano, F. M. Rojas, J. F. Rossier, and J. J. Palacios, Phys. Rev. B **81**, 165409 (2010).
- <sup>32</sup> G. Csányi, P. B. Littlewood, A. H. Nevidomskyy, C. J. Pickard, and B. D. Simons, Nature Physics **1**, 42 (2005).
- <sup>33</sup> I. I. Mazin, Phys. Rev. Lett. **95**, 227001 (2005).
- <sup>34</sup> M. Calandra and F. Mauri, Phys. Rev. B **74**, 094507 (2006).
- <sup>35</sup> D. Martoccia, et al., Phys. Rev. Lett. **101**, 126102 (2008).
- <sup>36</sup> G. Giovannetti, P. A. Khomyakov, G. Brocks, V. M. Karpan, J. van den Brink, and P. J. Kelly, Phys. Rev. Lett. **101**, 026803 (2008).
- <sup>37</sup> P. A. Khomyakov, G. Giovannetti, P. C. Rusu, G. Brocks, J. van den Brink, and P. J. Kelly, Phys. Rev. B **79**, 195425 (2009).
- <sup>38</sup> K. S. Novoselov, et. al., Science **306**, 666 (2004).
- <sup>39</sup> A. Das, et. al., Nature Nanotechnology **3**, 210 (2008).
- <sup>40</sup> O. V. Yazyev, Rep. Prog. Phys. **73**, 056501 (2010); and the references therein.
- <sup>41</sup> W. Kohn and L. J. Sham, Phys. Rev. **140**, A1133 (1965).
- <sup>42</sup> S. Baroni, S. de Gironcoli, A. Dal Corso, and P. Giannozzi, Rev. Mod. Phys. **73**, 515 (2001).
- <sup>43</sup> H. Eyring, J. Chem. Phys. **3**, 107 (1935).
- <sup>44</sup> P. Hänggi, P. Talkner, and M. Borkovec, Rev. Mod. Phys. **62**, 251 (1990).
- <sup>45</sup> E. Pollak and P. Talkner, Chaos **15**, 026116 (2005).
- <sup>46</sup> K. Toyoura, Y. Koyama, A. Kuwabara, F. Oba, and I. Tanaka, Phys. Rev. B **78**, 214303 (2008).
- <sup>47</sup> P. G. Sundell, M. E. Björketun, and G. Wahnström, Phys. Rev. B **76**, 094301 (2007).
- <sup>48</sup> Y. Ferro, D. Teillet-Billy, N. Rougeau, V. Sidis, S. morisset, and A. Allouche, Phys. Rev. B **78**, 085417 (2008).
- <sup>49</sup> P. Giannozzi et. al., J. Phys.: Condens. Matter **21**, 395502 (2009).
- <sup>50</sup> D. Vanderbilt, Phys. Rev. B **41**, R7892 (1990).
- <sup>51</sup> J. P. Perdew, K. Burke, and M. Ernzerhof, Phys. Rev. Lett. **77**, 3865 (1996).
- <sup>52</sup> G. Henkelman, B. P. Uberuage, and H. Jónsson, J. Chem. Phys. **113**, 9901 (2000).
- <sup>53</sup> R. S. Mulliken, J. Chem. Phys. **23**, 1833 (1955).
- <sup>54</sup> M. Y. Ni, L. F. Huang, L. J. Guo, and Z. Zeng, Int. J. Hydrogen Energy **35**, 3546 (2010).
- <sup>55</sup> J. A. Vergés and L. de Andres, Phys. Rev. B **81**, 075423 (2010).



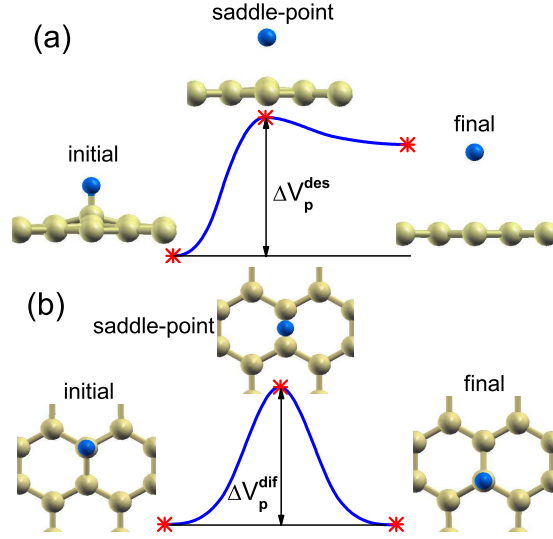


FIG. 1: (Color online) The MEPs for the (a) desorption and (b) diffusion of the hydrogen monomer on graphene. The initial, saddle-point (SP) and final states in the paths are labeled with stars, and their structures are shown alongside the graph. The yellow spheres are carbon atoms and the smaller blue spheres are hydrogen atoms. The final state in the desorption MEP is set to be the physisorption state.

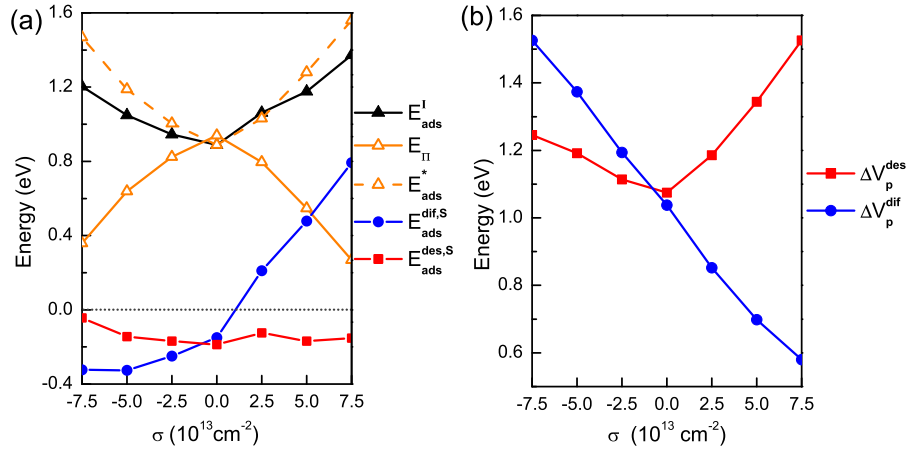


FIG. 2: (Color online) (a) The variations of  $E_{ads}^I$ ,  $E_{ads}^{des,S}$ ,  $E_{ads}^{dif,S}$ ,  $E_{II}$  and  $E_{ads}^*$  with respect to  $\sigma$ . (b) The variations of  $\Delta V_p^{des}$  and  $\Delta V_p^{dif}$  with respect to  $\sigma$ .

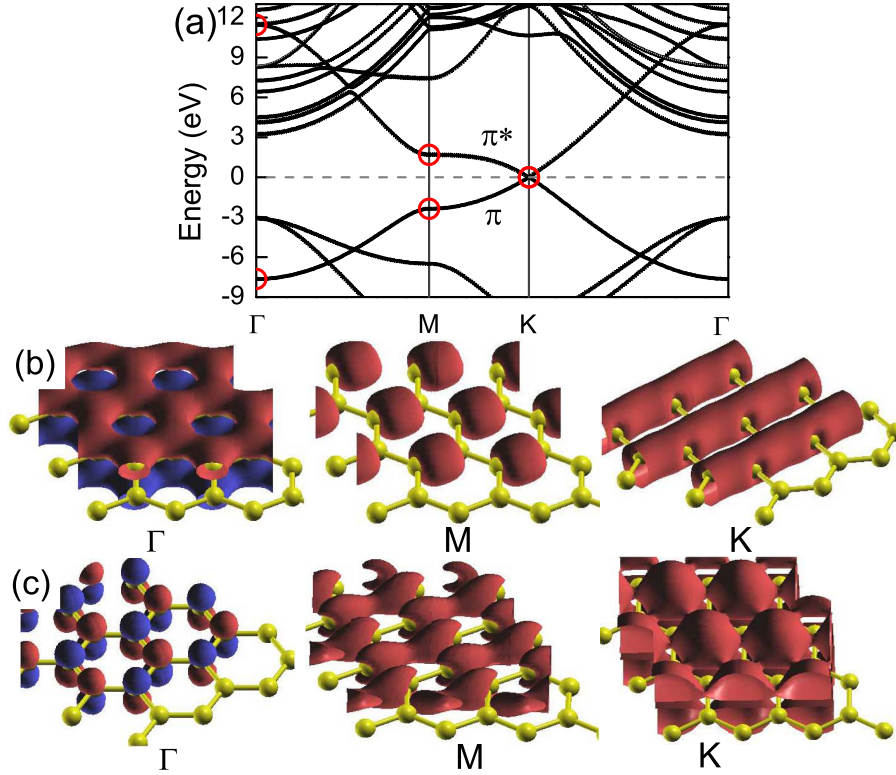


FIG. 3: (Color online) (a) The band structure of neutral graphene. The orbital shapes in real space of (b) the bonding  $\pi$  band and (c) the anti-bonding  $\pi^*$  band at  $\Gamma$ , M and K points. In (a), the bonding  $\pi$  band and the anti-bonding  $\pi^*$  band at  $\Gamma$ , M and K points are each labeled with a red circle.

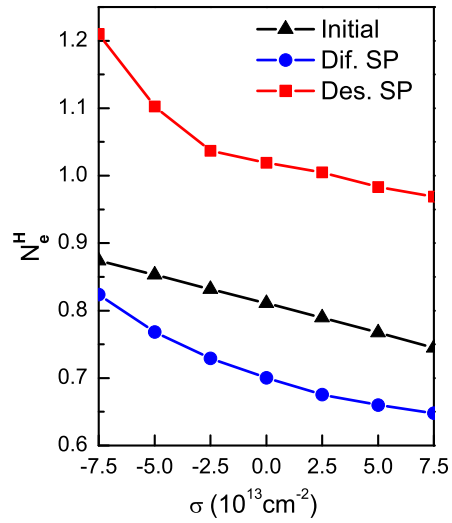


FIG. 4: (Color online) The variations of  $N_e^H$ s in the initial, desorption SP and diffusion SP states with respect to  $\sigma$ .

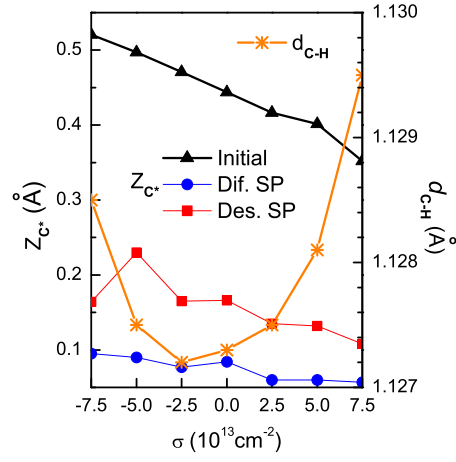


FIG. 5: (Color online) The variations of  $d_{C-H}$  in the initial state and  $Z_{C^*}$ s in the initial, desorption SP and diffusion SP states with respect to  $\sigma$ .

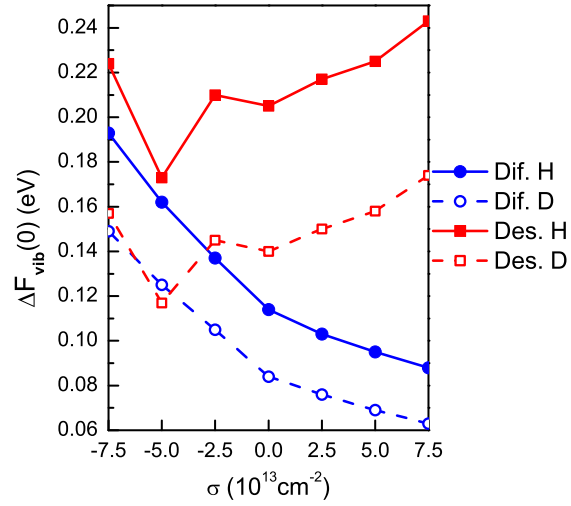


FIG. 6: (Color online) The variations of the  $\Delta F_{vib}(0)$ s for the desorption and diffusion of H and D monomers on graphene with respect to  $\sigma$ .

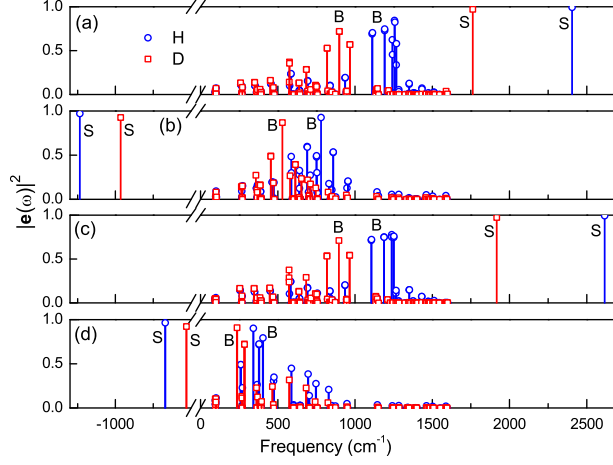


FIG. 7: (Color online) The calculated spectra of  $|e(\omega_i)|^2$  ( $i$  is the index of the vibrational mode) of H (D) monomer in (a) the initial state and (b) the desorption SP state at  $\sigma$  of  $-5.0 \times 10^{13} \text{ cm}^{-2}$ , and in (c) the initial state and (d) the desorption SP state at  $\sigma$  of  $-7.5 \times 10^{13} \text{ cm}^{-2}$ .

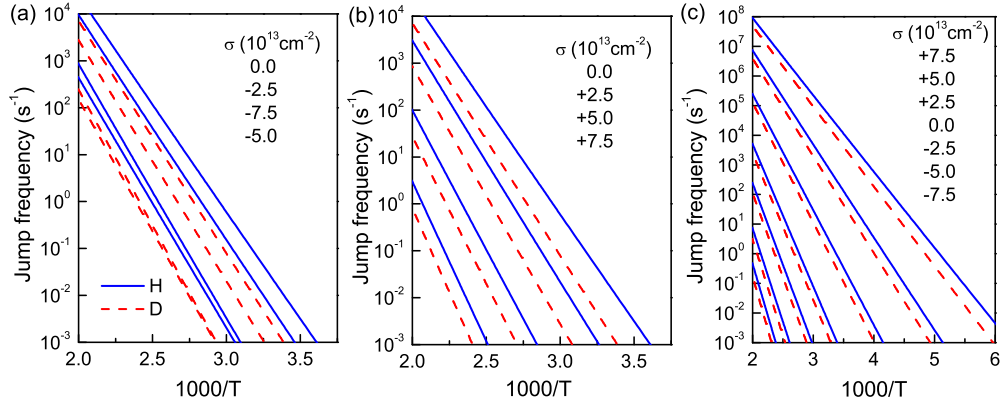


FIG. 8: (Color online) The variations of the jump frequencies for the (a, b) desorption and (c) diffusion of H and D monomers on graphene at various  $\sigma$ s with respect to the inverse of temperature.

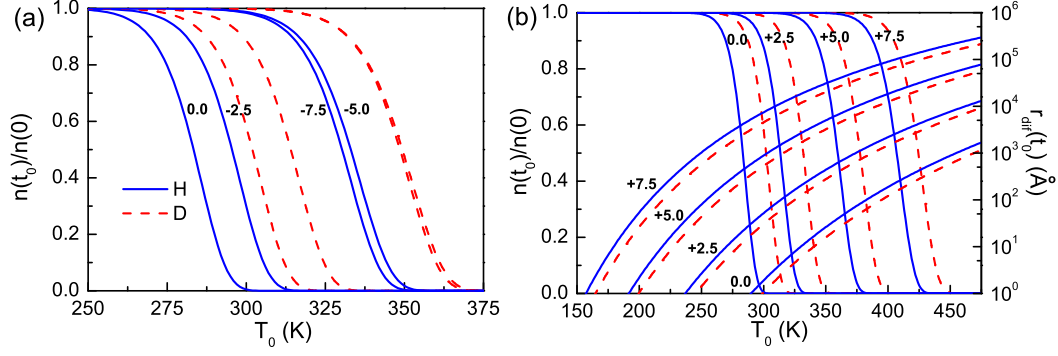


FIG. 9: (Color online) The variations of the  $n(t_0)/n(0)$ s and  $r_{dif}(t_0)$ s for H and D monomers at various  $\sigma$ s with respect to the annealing temperature ( $T_0$ ) in the annealing process ( $t_0 = 300s$ ). The  $r_{dif}(t_0)$ s at negative  $\sigma$ s are not shown, because the diffusion of H (D) monomer is stopped by electron doping.

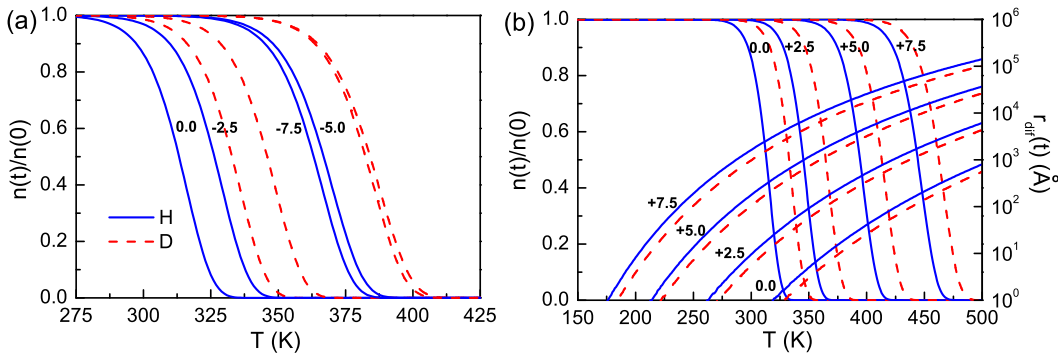


FIG. 10: (Color online) The variations of the  $n(t)/n(0)$ s and  $r_{dif}(t)$ s for H and D monomers at various  $\sigma$ s with respect to temperature in the constant-rate heating process ( $\alpha = 1.0$  K/s). The  $r_{dif}(t)$ s at negative  $\sigma$ s are not shown, because the diffusion of H (D) monomer is stopped by electron doping.

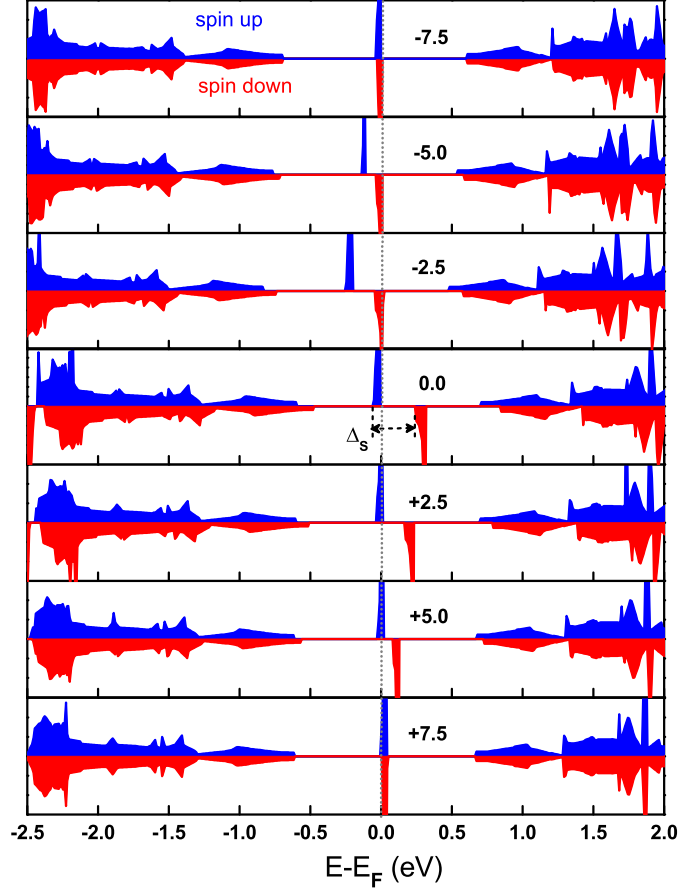


FIG. 11: (Color online) The electronic DOS for the chemisorption states at various  $\sigma$ s. The gray vertical dotted line at the Fermi level guides the eyes. The definition of  $\Delta_s$  is shown in the DOS spectrum at  $\sigma = 0.0$ .

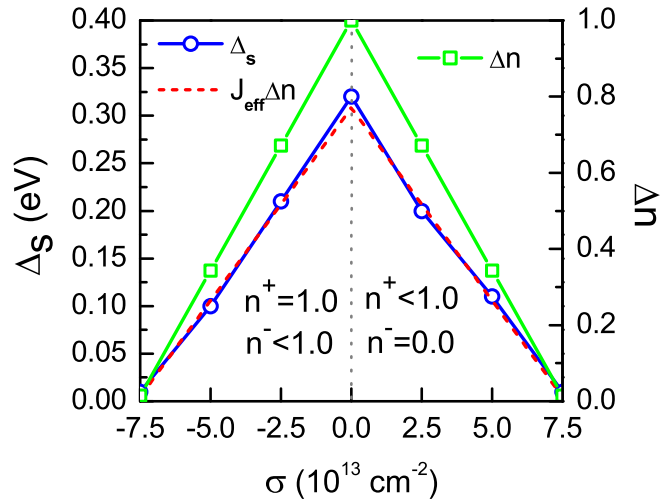


FIG. 12: (Color online) The variation of  $\Delta_n$ ,  $\Delta_s$  and  $\frac{1}{4}J_{eff}\Delta_n$  with respect to  $\sigma$ .  $J_{eff}$  is fitted to be 1.23 eV.